Inorganic Chemistry

Article

pubs.acs.org/IC

Microwave-Assisted Synthesis of a Series of Lanthanide Metal–Organic Frameworks and Gas Sorption Properties

Zu-Jin Lin,[†,‡] Zhen Yang,[†,‡] Tian-Fu Liu,[†] Yuan-Biao Huang,[†] and Rong Cao*[,†]

[†]State Key Laboratory of Structural Chemistry, Fujian Institute of Research on the Structure of Matter, Chinese Academy of Sciences, Fujian, Fuzhou 350002, P. R. China;

[‡]Graduate School of the Chinese Academy of Sciences, Beijing 100039, P. R. China

Supporting Information

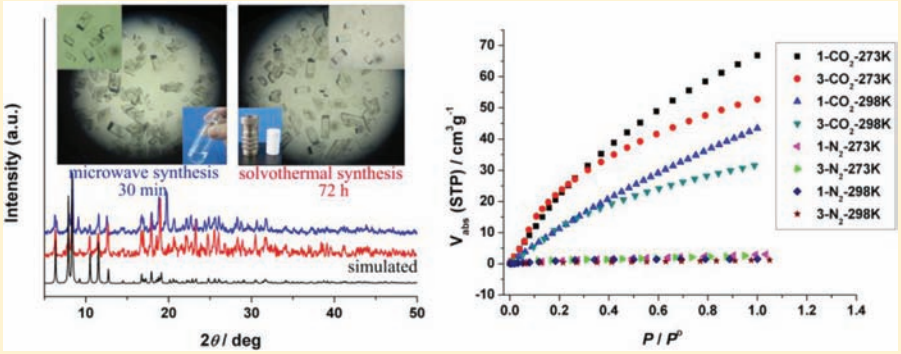

ABSTRACT: A series of isostructural microporous lanthanide metal–organic frameworks (MOFs) formulated as $[Ln_2(TPO)_2(HCOO)]\cdot(Me_2NH_2)\cdot(DMF)_4\cdot(H_2O)_6$ {Ln = Y (**1**), Sm (**2**), Eu (**3**), Gd (**4**), Tb (**5**), Dy (**6**), Ho (**7**), Er (**8**), Tm (**9**), Yb (**10**), and Lu (**11**); H_3TPO = tris-(4-carboxylphenyl)phosphineoxide; DMF = *N*,*N*-dimethylformamide} has been synthesized under microwave-assisted solvothermal reaction for 30 min. Alternatively, if a conventional solvothermal reaction is carried out under the same temperature, a much longer time (3 days) is needed for the same phase in similar yield. Structure analysis reveals that the framework is a 4,8-connected network with point symbol $(4^{10}\cdot6^{16}\cdot8^2)$ $(4^5\cdot6)^2$, which is the subnet of ***alb*** net. Thermal gravimetric analyses performed on as-synthesized MOFs reveal that the frameworks have high thermal stability. The luminescent properties of **2**, **3**, **5**, and **6** were investigated and show characteristic emissions for Sm(III), Eu(III), Tb(III), and Dy(III) at room temperature, respectively. Gas sorption properties of **1** and **3** were studied by experimentally measuring nitrogen, argon, carbon dioxide, methane, and hydrogen sorption isotherms. The resulting materials show high and preferential CO_2 adsorption over N_2 gas at ambient temperature, indicating that the present materials can be applied in a CO_2 capture process.

INTRODUCTION

Microporous metal–organic frameworks (MOFs) are emerging as an important family of porous materials.[1] Owing to their permanent porosity, high surface areas, fine-tunable pore structures, and adjustable chemical functionalities, they have been studied for applications in gas storage and separation, such as hydrogen/methane storage and carbon dioxide capture.[2] Among the diverse metal–organic frameworks, lanthanide-based metal–organic frameworks are attractive owning to their characteristic coordination preferences and unique optical and magnetic properties arising from 4f electrons. Compared to the first-row transition metal ions, lanthanide ions have larger coordination spheres and more flexible coordination geometries. In principle, these characteristics result in more facile routes to densely packed solids. Some lanthanide MOFs possess open frameworks, but collapse or become amorphous after guest removal, even if they exhibit reversible solvent exchange.[3] So far, many searches for reported lanthanide MOFs have focused on magnetic and photoluminescent properties;[4] it is still challenging to construct porous lanthanide MOFs with permanent porosity and to develop their potential application in gas adsorption and separation.[5]

So far, metal–organic frameworks are predominantly synthesized under hydrothermal/solvothermal condition which usually requires long reaction times (days to weeks) and heavy energy consumption. Development of facile, rapid, and economical routes for the syntheses of MOFs has been a challenging task for practical applications. Generally, microwave synthesis can dramatically reduce the reaction time and enhance product yields. This simple and energy-efficient heating process has been successfully used in organic synthesis[6] and in the preparation of nanoporous inorganic materials.[7] Just recently, the method has also been applied to prepare metal

Received: September 27, 2011
Published: January 5, 2012

   dx.doi.org/10.1021/ic202082w | *Inorg. Chem.* 2012, 51, 1813–1820

clusters[8] and MOFs with known structures.[9] Because of the fast kinetics of crystal nucleation and growth, microsized crystals of MOFs are often prepared under microwave heating. Although some novel coordination polymers were prepared by microwave method through careful design of the synthetic conditions,[10] the application of microwave method in the preparation of novel functional MOFs is still limited.

Herein, we report the microwave-assisted solvothermal synthesis and sorption properties of a series of isostructural three-dimensional (3D) lanthanide MOFs formulated as $[Ln_2(TPO)_2(HCOO)]\cdot(Me_2NH_2)\cdot(DMF)_4\cdot(H_2O)_6$ [Ln = Y (**1**), Sm (**2**), Eu (**3**), Gd (**4**), Tb (**5**), Dy (**6**), Ho (**7**), Er (**8**), Tm (**9**), Yb (**10**), and Lu (**11**); H_3TPO = tris(4-carboxylphenyl)phosphineoxide]. We present the syntheses and detailed structure descriptions of the 11 isostructural MOFs along with the topology studies. Besides, we have studied the solid-state emission spectra of **2**, **3**, **5**, and **6**. Furthermore, we also illustrated the pore characteristics and gas sorption properties of **1** and **3** by experimentally measuring nitrogen, argon, carbon dioxide, methane, and hydrogen sorption isotherms.

EXPERIMENTAL SECTION

Materials and General Methods. All chemicals purchased were of reagent grade and used without further purification. The ligand H_3PTO was synthesized according to literature.[5g,11] Microwave-assisted solvothermal syntheses were carried out in a microwave oven (Initiator 8 EXP, 2450 MHz frequency, Biotage Corp.). Elemental analyses (C, H, and N) were carried out on an Elementar Vario EL III analyzer. Infrared (IR) spectra were recorded on PerkinElmer Spectrum One with KBr pellets in the range 4000−400 cm^{-1}. Powder X-ray diffraction (PXRD) data were collected on a Rigaku MiniFlex2 diffractometer working with Cu Kα radiation, and the recording speed was 5° min^{-1} over the 2θ range of 5−50° at room temperature. Thermogravimetric analyses (TGA) were performed under a nitrogen atmosphere with a heating rate of 10 °C/min using an SDT Q600 thermogravimetric analyzer. ^1H NMR spectra were recorded at ambient temperature on a Bruker Avance III spectrometer; the chemical shifts were referenced to TMS in the solvent signal in d_6-DMSO. Fluorescence spectroscopy data were recorded on a FLS920 fluorescence spectrophotometer. The simulated powder patterns were calculated using Mercury 2.0. The purity and homogeneity of the bulk products were determined by comparison of the simulated and experimental X-ray powder diffraction patterns.

Synthesis of $[Y_2(TPO)_2(HCOO)]\cdot(Me_2NH_2)\cdot(DMF)_4\cdot(H_2O)_6$ (1). $Y(NO_3)_3\cdot6H_2O$ (0.10 mmol, 38 mg), H_3TPO (0.10 mmol, 41 mg), a mixed solvent (7 mL, DMF/H_2O/EtOH = 3:3:1) and 0.5 mL of CH_3COOH were placed together in a 30 mL microwave tube. The mixture was heated by microwave under autogenous pressure at 105 °C for 0.5 h, and then cooled naturally to room temperature. Colorless block crystals suitable for single-crystal X-ray diffraction were obtained by filtration, washed for several times with DMF/H_2O/EtOH (3:3:1), and dried in air at ambient temperature. The compound can also be synthesized by a conventional solvothermal reaction at the same temperature for 3 days. The compound is stable in air and insoluble in common organic solvents such as methanol, ethanol, acetonitrile, acetone, dimethylsulfoxide, and DMF. Yield: 80% (based on H_3TPO). Anal. Calcd for $C_{58}H_{74}N_5O_{28}P_2Y_2$ (M_r = 1528.21): C, 45.56; H, 4.88; N, 4.58. Found: C, 45.50; H, 4.83; N, 4.56. IR (KBr): ν = 3430(br), 3061(m), 2933(m), 2810 (w), 1666(s), 1588(s), 1533(s), 1497(m), 1417(s), 1162(s), 1111(s), 1019(m), 855(m), 777(m), 740(s), 700(m), 583(m), 488(m).

Synthesis of $[Sm_2(TPO)_2(HCOO)]\cdot(Me_2NH_2)\cdot(DMF)_4\cdot(H_2O)_6$ (2). The procedure was the same as that for compound **1** except that $Y(NO_3)_3\cdot6H_2O$ was replaced by $Sm(NO_3)_3\cdot6H_2O$. Yield: 75% (based on H_3TPO). Anal. Calcd for $C_{58}H_{74}N_5O_{28}P_2Sm_2$ (M_r = 1651.89): C, 42.17; H, 4.52; N, 4.24. Found: C, 42.07; H, 4.43; N, 4.21. IR (KBr): ν = 3418(br), 3060(m), 2931(m), 2808(w), 1666(s), 1588(s), 1532(s), 1498(m), 1415(s), 1164(s), 1112(s), 1017(m), 855(m), 777(m), 742(s), 700(m), 581(m), 489(m).

Synthesis of $[Eu_2(TPO)_2(HCOO)]\cdot(Me_2NH_2)\cdot(DMF)_4\cdot(H_2O)_6$ (3). The procedure was the same as that for compound **1** except that $Y(NO_3)_3\cdot6H_2O$ was replaced by $Eu(NO_3)_3\cdot6H_2O$. Yield: 73% (based on H_3TPO). Anal. Calcd for $C_{58}H_{74}N_5O_{28}P_2Eu_2$ (M_r = 1656.24): C, 42.09; H, 4.51; N, 4.23. Found: C, 42.11; H, 4.48; N, 4.17. ν = 3422(br), 3062(m), 2931(m), 2808(w), 1664(s), 1588(s), 1532(s), 1499(m), 1415(s), 1163(s), 1112(s), 1017(m), 856(m), 778(m), 742(s), 700(m), 581(m), 489(m).

Synthesis of $[Gd_2(TPO)_2(HCOO)]\cdot(Me_2NH_2)\cdot(DMF)_4\cdot(H_2O)_6$ (4). The procedure was the same as that for compound **1** except that $Y(NO_3)_3\cdot6H_2O$ was replaced by $Gd(NO_3)_3\cdot6H_2O$. Yield: 79% (based on H_3TPO). Anal. Calcd for $C_{58}H_{74}N_5O_{28}P_2Gd_2$ (M_r = 1666.25): C, 41.82; H, 4.48; N, 4.20. Found: C, 41.78; H, 4.40; N, 4.14. ν = 3418(br), 3060(m), 2930(m), 2808(w), 1661(s), 1589(s), 1532(s), 1498(m), 1416(s), 1165(s), 1112(s), 1017(m), 858(m), 778(m), 744(s), 700(m), 581(m), 489(m).

Synthesis of $[Tb_2(TPO)_2(HCOO)]\cdot(Me_2NH_2)\cdot(DMF)_4\cdot(H_2O)_6$ (5). The procedure was the same as that for compound **1** except that $Y(NO_3)_3\cdot6H_2O$ was replaced by $Tb(NO_3)_3\cdot6H_2O$. Yield: 81% (based on H_3TPO). Anal. Calcd for $C_{58}H_{74}N_5O_{28}P_2Tb_2$ (M_r = 1668.25): C, 41.74; H, 4.47; N, 4.20. Found: C, 41.77; H, 4.42; N, 4.17. ν = 3417(br), 3062(m), 2931(w), 2808(m), 1661(s), 1588(s), 1532(s), 1499(m), 1416(s), 1164(s), 1112(s), 1017(m), 859(m), 778(m), 744(s), 700(m), 581(m), 489(m).

Synthesis of $[Dy_2(TPO)_2(HCOO)]\cdot(Me_2NH_2)\cdot(DMF)_4\cdot(H_2O)_6$ (6). The procedure was the same as that for compound **1** except that $Y(NO_3)_3\cdot6H_2O$ was replaced by $Dy(NO_3)_3\cdot6H_2O$. Yield: 82% (based on H_3TPO). Anal. Calcd for $C_{58}H_{74}N_5O_{28}P_2Dy_2$ (M_r = 1678.26): C, 41.56; H, 4.45; N, 4.18. Found: C, 41.53; H, 4.41; N, 4.11. ν = 3394(br), 3059(m), 2930(w), 1668(s), 1591(s), 1535(s), 1498(m), 1418(s), 1169(s), 1113(s), 1017(m), 858(m), 777(m), 744(s), 700(m), 581(m), 489(m).

Synthesis of $[Ho_2(TPO)_2(HCOO)]\cdot(Me_2NH_2)\cdot(DMF)_4\cdot(H_2O)_6$ (7). The procedure was the same as that for compound **1** except that $Y(NO_3)_3\cdot6H_2O$ was replaced by $Ho(NO_3)_3\cdot6H_2O$. Yield: 82% (based on H_3TPO). Anal. Calcd for $C_{58}H_{74}N_5O_{28}P_2Ho_2$ (M_r = 1680.26): C, 41.44; H, 4.44; N, 4.17. Found: C, 41.43; H, 4.51; N, 4.12. ν = 3410(br), 3060(m), 2930(w), 1663(s), 1589(s), 1532(s), 1498(m), 1417(s), 1165(s), 1113(s), 1017(m), 856(m), 777(m), 744(s), 700(m), 581(m), 489(m).

Synthesis of $[Er_2(TPO)_2(HCOO)]\cdot(Me_2NH_2)\cdot(DMF)_4\cdot(H_2O)_6$ (8). The procedure was the same as that for compound **1** except that $Y(NO_3)_3\cdot6H_2O$ was replaced by $Er(NO_3)_3\cdot6H_2O$. Yield: 85% (based on H_3TPO). Anal. Calcd for $C_{58}H_{74}N_5O_{28}P_2Er_2$ (M_r = 1682.26): C, 41.33; H, 4.42; N, 4.15. Found: C, 41.32; H, 4.47; N, 4.16. ν = 3413(br), 3060(m), 2932(w), 1665(s), 1591(s), 1535(s), 1496(m), 1416(s), 1163(s), 1111(s), 1018(m), 860(m), 777(m), 744(s), 700(m), 581(m), 489(m).

Synthesis of $[Tm_2(TPO)_2(HCOO)]\cdot(Me_2NH_2)\cdot(DMF)_4\cdot(H_2O)_6$ (9). The procedure was the same as that for compound **1** except that $Y(NO_3)_3\cdot6H_2O$ was replaced by $Tm(NO_3)_3\cdot6H_2O$. Yield: 80% (based on H_3TPO). Anal. Calcd for $C_{58}H_{74}N_5O_{28}P_2Tm_2$ (M_r = 1688.27): C, 41.24; H, 4.42; N, 4.15. Found: C, 41.18; H, 4.44; N, 4.10. ν = 3390(br), 3056(m), 2937(w), 1670(s), 1588(s), 1536(s), 1499(m), 1418(s), 1162(s), 1117(s), 1016(m), 852(m), 777(m), 744(s), 700(m), 581(m), 489(m).

Synthesis of $[Yb_2(TPO)_2(HCOO)]\cdot(Me_2NH_2)\cdot(DMF)_4\cdot(H_2O)_6$ (10). The procedure was the same as that for compound **1** except that $Y(NO_3)_3\cdot6H_2O$ was replaced by $Yb(NO_3)_3\cdot6H_2O$. Yield: 70% (based on H_3TPO). Anal. Calcd for $C_{58}H_{74}N_5O_{28}P_2Yb_2$ (M_r = 1698.28): C, 41.04; H, 4.39; N, 4.13. Found: C, 41.03; H, 4.35; N, 4.06. ν = 3420(br), 3063(m), 2933(w), 1669(s), 1591(s), 1533(s), 1496(m), 1417(s), 1170(s), 1110(s), 1015(m), 858(m), 777(m), 744(s), 700(m), 581(m), 489(m).

Synthesis of $[Lu_2(TPO)_2(HCOO)]\cdot(Me_2NH_2)\cdot(DMF)_4\cdot(H_2O)_6$ (11). The procedure was the same as that for compound **1** except that $Y(NO_3)_3\cdot6H_2O$ was replaced by $Lu(NO_3)_3\cdot6H_2O$. Yield: 74%

dx.doi.org/10.1021/ic202082w | Inorg. Chem. 2012, 51, 1813−1820

Table 1. Crystal Data[a] and Structure Refinement of 1−5

	1-Y	2-Sm	3-Eu	4-Gd	5-Tb
formula	$C_{43}H_{25}O_{16}P_2Y_2$	$C_{43}H_{25}O_{16}P_2Sm_2$	$C_{43}H_{25}O_{16}P_2Eu_2$	$C_{43}H_{25}O_{16}P_2Gd_2$	$C_{43}H_{25}O_{16}P_2Tb_2$
fw	1037.39	1160.27	1163.49	1174.07	1177.41
cryst syst	monoclinic	monoclinic	monoclinic	monoclinic	monoclinic
space group	*P*2/*c*	*P*2/*c*	*P*2/*c*	*P*2/*c*	*P*2/*c*
a/Å	14.539(4)	14.664(3)	14.617(3)	14.528(3)	14.617(4)
b/Å	10.546(3)	10.603(2)	10.572(2)	10.497(2)	10.572(3)
c/Å	23.378(6)	23.698(4)	23.548(5)	23.674(8)	23.548(7)
α/deg	90.00	90.00	90.00	90.00	90.00
β/deg	107.231(5)	108.058(10)	107.79(3)	107.97(3)	107.787(4)
γ/deg	90.00	90.00	90.00	90.00	90.00
unit cell volume/Å^3	3423.8(16)	3503.1(11)	3465.0(12)	3434.2(15)	3465.0(16)
Z	2	2	2	2	2
μ/mm^{-1}	1.779	1.750	1.885	2.006	2.115
data measured	26 188	26 888	26 693	28 856	26 623
unique data	7807	8029	7895	7859	7909
R_{int}	0.0779	0.0458	0.0554	0.0459	0.0469
GOF	0.995	1.139	1.018	1.086	1.079
R_1[b] ($I > 2\sigma(I)$)	0.0566	0.0674	0.0340	0.0355	0.0399
$wR(F^2)$[c] ($I > 2\sigma(I)$)	0.1582	0.2070	0.0968	0.0884	0.1115
R_1[b] (all data)	0.0799	0.0724	0.0421	0.0403	0.0451
$wR(F^2)$[c] (all data)	0.1749	0.2142	0.0997	0.0908	0.1182
CCDC number	818 479	818 482	818 483	818 484	818 485

[a]Obtained with graphite-monochromated Mo K*α* (λ = 0.710 73 Å) radiation. [b]$R_1 = \sum||F_o| - |F_c||/\sum|F_o|$. [c]$wR_2 = \{\sum[w(F_o^2 - F_c^2)^2]/\sum[w(F_o^2)^2]\}^{1/2}$.

Table 2. Crystal Data[a] and Structure Refinement of 6−11

	6-Dy:	7-Ho:	8-Er:	9-Tm:	10-Yb:	11-Lu
chemical formula	$C_{43}H_{25}O_{16}P_2\ Dy_2$	$C_{43}H_{25}O_{16}P_2\ Ho_2$	$C_{43}H_{25}O_{16}P_2\ Er_2$	$C_{43}H_{25}O_{16}P_2\ Tm_2$	$C_{43}H_{25}O_{16}P_2\ Yb_2$	$C_{43}H_{25}O_{16}P_2\ Lu_2$
formula mass	1184.57	1189.43	1194.09	1197.43	1205.65	1209.51
cryst syst	monoclinic	monoclinic	monoclinic	monoclinic	monoclinic	monoclinic
space group	*P*2/*c*	*P*2/*c*	*P*2/*c*	*P*2/*c*	*P*2/*c*	*P*2/*c*
a/Å	14.617(4)	14.4523(11)	14.4248(11)	14.4014(11)	14.3832(11)	14.4262(11)
b/Å	10.572(3)	10.4767(5)	10.4553(5)	10.4577(5)	10.4548(5)	10.4932(5)
c/Å	23.548(7)	23.4337(18)	23.4323(18)	23.3524(18)	23.3057(18)	23.2269(18)
α/deg	90.00	90.00	90.00	90.00	90.00	90.00
β/deg	107.787(4)	107.577(4)	107.501(4)	107.371(4)	107.348(4)	107.052(4)
γ/deg	90.00	90.00	90.00	90.00	90.00	90.00
unit cell volume/Å^3	3465.0(16)	3382.5(4)	3370.4(4)	3356.6(4)	3345.1(4)	3361.5(4)
Z	2	2	2	2	2	2
μ/mm^{-1}	2.231	2.415	2.566	2.720	2.873	3.014
data measured	26 328	28 566	28 609	28 444	28 418	25 992
unique data	7874	7735	7683	7683	7662	7696
R_{int}	0.0430	0.0338	0.0722	0.0578	0.0461	0.0462
GOF	1.083	1.084	1.081	1.130	1.118	1.048
R_1[b] ($I > 2\sigma(I)$)	0.0378	0.0315	0.0590	0.0509	0.0469	0.0384
$wR(F^2)$[c] ($I > 2\sigma(I)$)	0.1091	0.0949	0.1850	0.1719	0.1716	0.1115
R_1[b] (all data)	0.0417	0.0349	0.0707	0.0609	0.0537	0.0443
$wR(F^2)$[c] (all data)	0.1119	0.0968	0.1941	0.1788	0.1771	0.1153
CCDC number	818 486	818 487	818 488	818 489	818 480	818 481

[a]Obtained with graphite-monochromated Mo K*α* (λ = 0.710 73 Å) radiation. [b]$R_1 = \sum||F_o| - |F_c||/\sum|F_o|$. [c]$wR_2 = \{\sum[w(F_o^2 - F_c^2)^2]/\sum[w(F_o^2)^2]\}^{1/2}$.

(based on H_3TPO). Anal. Calcd for $C_{58}H_{74}N_5O_{28}P_2Lu_2$ (M_r = 1700.28): C, 40.95; H, 4.38; N, 4.12. Found: C, 41.05; H, 4.33; N, 4.08. *ν* = 3324(br), 3066(m), 2938(w), 1668(s), 1593(s), 1537(s), 1493(m), 1415(s), 1162(s), 1117(s), 1016(m), 858(m), 777(m), 744(s), 700(m), 581(m), 489(m).

Single-Crystal X-ray Crystallography. Single-crystal X-ray diffraction data of compounds **1**−**6** were collected on a Rigaku Mercury CCD diffractometer with graphite monochromatized Mo K*α* radiation (λ = 0.710 73 Å), and the diffraction data of **7**−**11** were collected on a Rigaku Saturn 724+ diffractometer equipped with graphite monochromatized Mo K*α* radiation (λ = 0.710 73 Å) and a CCD area detector. All absorption corrections were performed using the *CrystalClear* program.[12] The structures were solved by direct methods and refined by the full matrix least-squares on F^2 using the SHELXTL-97 program package.[13] All non-hydrogen atoms were refined with anisotropic displacement parameters. The positions of

dx.doi.org/10.1021/ic202082w | *Inorg. Chem.* 2012, 51, 1813−1820

hydrogen atoms attached to carbon atoms were generated geometrically. Attempts to locate and model the highly disordered solvent molecules in the pores were unsuccessful. Therefore, the SQUEEZE routine of PLATON was used to remove the diffraction contribution from these solvents to produce a set of solvent free diffraction intensities.[14] Details of the structure solution and final refinements for the compounds were given in Tables 1 and 2. Selected bond lengths and angles for **1**−**11** were listed in Tables S1−11 in the Supporting Information. CCDC 818479−818489 contain the crystallographic data for this paper. These data can be obtained free of charge from the Cambridge Crystallographic Date Center via www.ccdc.cam.ac.uk.

Gas Adsorption Measurements. Low-pressure gas adsorption measurements were carried out on an ASAP (accelerated surface area and porosimetry) 2020 system. High-pressure carbon dioxide adsorption measurements were carried out on a hydrogen storage analyzer HTP1-V instrument. High-pressure hydrogen and methane adsorption measurements were carried out on an intelligent gravimetric sorption analyzer IGA100B instrument. The desolvated samples were prepared as follows: A fresh sample was soaked in methanol for 24 h, and the extract was discarded. Fresh methanol was subsequently added, and the sample was allowed to soak for another 24 h to remove DMF and H_2O solvates. The sample was then treated with dichloromethane in the same procedures to remove methanol solvates; after the removal of dichloromethane by decanting, the sample was dried under a dynamic vacuum ($<10^{-3}$ Torr) at 373 K for 10 h. Before gas adsorption measurement, the sample was dried again by using the "outgas" function of the surface area analyzer for 5 h at 373 K. The measurements were maintained at 77, 87, 195, and 273 K with a liquid nitrogen bath, a liquid argon bath, an acetone−dry ice bath, and an ice−water bath, respectively.

Syntheses and Crystal Structures. Compounds **1**−**11** were synthesized by microwave heating at 105 °C for 30 min. Alternatively, if a conventional solvothermal reaction in a Teflon-lined autoclave is carried out, a much longer time (105 °C, 3 days) is needed for the same phase in similar yield. The crystals synthesized by microwave heating have similar sizes and shapes to those obtained by conventional solvothermal method (Figure 1), while the microwave

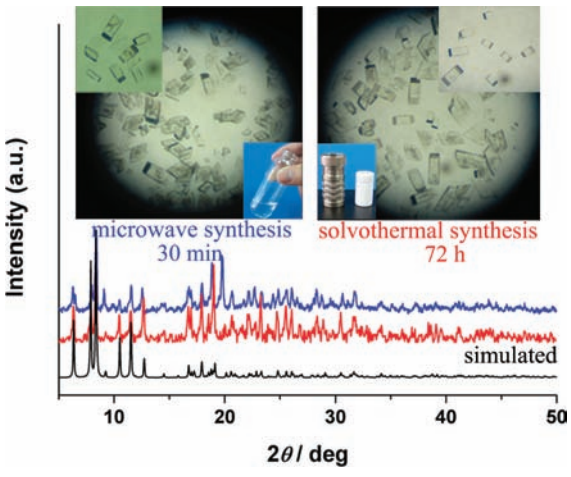

Figure 1. Comparison of complexes prepared under microwave heating and conventional solvothermal synthesis.

heating is more efficient and less of an energy consumer. Although formate ions are found in the structures, acetic acid plays a crucial role in the formation of the target frameworks. The preparation of the frameworks failed if acetic acid was replaced by formic acid in the reaction; when a small amount of HNO_3 was added to the reaction mixture instead of acetic acid under the same solvothermal reaction conditions, other compounds were obtained, which were reported previously.[5g]

The single-crystal X-ray diffraction studies performed on **1**−**11** reveal that all 11 compounds are 3D frameworks, crystallizing in the monoclinic space group *P*2/*c*. Because they are isostructural, herein, only the structure of **3** will be described in detail as a representative. Each asymmetric unit of **3** contains one crystallographically independent europium ion, one TPO^{3-} ligand, and 0.5 formate anion (Figure 2b). The two adjacent europium centers are triply bridged by one formate anion and two carboxylate groups from two TPO^{3-} ligands, leading to the construction of a binuclear europium cluster $[Eu_2O_2(COO)_6(HCOO)]$. In the structure, every TPO^{3-} ligand links four binuclear europium clusters, and every binuclear europium cluster connects eight TPO^{3-} ligands, thus forming a 3D 4,8-connected binodal net with point symbol $(4^{10}.6^{16}.8^2)(4^5.6)^2$. This net is derived from analyzing supernet-subnet relations by TOPOS and is a subnet of the ***alb*** net (Figure 2d).[15] In contrast to other neutral lanthanide MOFs, compound **3** exhibits a negatively charged network with $H_2N(CH_3)_2^+$ counterion residing in the channels, which was confirmed by ^1H NMR spectrum (Figure S2). The formate anion and $NH_2(CH_3)_2^+$ may be generated via either hydrolysis or decarbonylation of DMF under microwave heating/solvothermal condition.[16] The distances between the europium(III) and carboxylate oxygen range from 2.299(3) to 2.516(3) Å, which are comparable to those reported for other europium−oxygen donor complexes.[3b] A close inspection of the solvent-accessible surface discloses that straight open channels are present along the crystallographic axes. Taking into account the van der Waals surface of the backbone, the passage windows in **3** are estimated to be 3.9 × 4.7 Å^2, 3.9 × 6.0 Å^2, 7.7 × 7.7 Å^2 (and 3.7 × 3.7 Å^2) along *a*-, *b*- (Figure S7), and *c*-axes (Figure 2c), respectively. The solvent accessible void volume is about 43.1% after removal of the disordered solvent molecules, as estimated using PLATON.[14]

Thermal Stability Analysis. To investigate their thermal stabilities, thermal gravimetric analyses (TGA) were performed on a STQ 600 instrument. As shown in Figure S5, because these compounds are isostructural, they show similar thermal stability and are stable at least up to 200 °C. The continuous weight losses from 30 °C to ∼280 °C correspond to the loss of all guest molecules (6 H_2O and 4 DMF), which is followed by a steady plateau up to 480 °C. The frameworks start to burn off with the loss of TPO^{3-} ligands above 480 °C. The thermal stabilities of **1**−**11** showed from TGA curves are comparable to that of the highest of reported porous MOFs.[5c,e,g]

Adsorption Properties. Because of the isostructural frameworks of **1**−**11**, with the atomic number of lanthanide cations increasing from Y to Lu, the molecular mass becomes larger; therefore, it is reasonable to expect that the gravimetric adsorption capacities tend to gradually decrease from compound **1** (Y) to **11** (Lu). As a representative, only the sorption properties of **1** (smallest formula weight) and **3** (medium formula weight) will be studied in detail. The desolvated samples were prepared by solvent exchange and then degassed under ultrahigh vacuum at 100 °C for 15 h (Experimental Section). The complete elimination of the DMF molecules in the desolvated samples were confirmed by the IR spectra where the characteristic C=O stretching of DMF disappeared (Figure S1). The PXRD patterns for desolvated samples are similar to that of the as-synthesized samples, indicating that the departure of the guest molecules does not lead to an obvious phase transformation (Figure S4).

The permanent porosity of the desolvated samples was confirmed by N_2 sorption experiments at 77 K. As shown in Figure 3, N_2 adsorption isotherms of the two fully activated MOFs reveal typical type-I behaviors as expected for microporous materials. Nitrogen adsorption indicates a surface area of 1011.2 m^2 g^{-1} for **1** and 725.2 m^2 g^{-1} for **3** using a Langmuir model, respectively. Application of the standard Brunauer−Emmett−Teller (BET) model for N_2 adsorption gave the measured surface areas of 692.0 m^2 g^{-1} for **1** and 495.5 m^2 g^{-1} for **3**, with the corresponding estimated micropore volume of 0.33 mL g^{-1} and 0.23 mL g^{-1} (*t*-plot analysis), respectively. The pore size distribution derived from the N_2 adsorption isotherms using the Horvath−Kawazoe (HK) method suggests that both **1** and **3** have two main pores with sizes of 3.6 and 4.2 Å. The result is consistent with the isostructural character of the complexes. Due to the disorder of $H_2N(CH_3)_2^+$ in the channels, the pore size values are smaller than

dx.doi.org/10.1021/ic202082w | *Inorg. Chem.* 2012, 51, 1813−1820

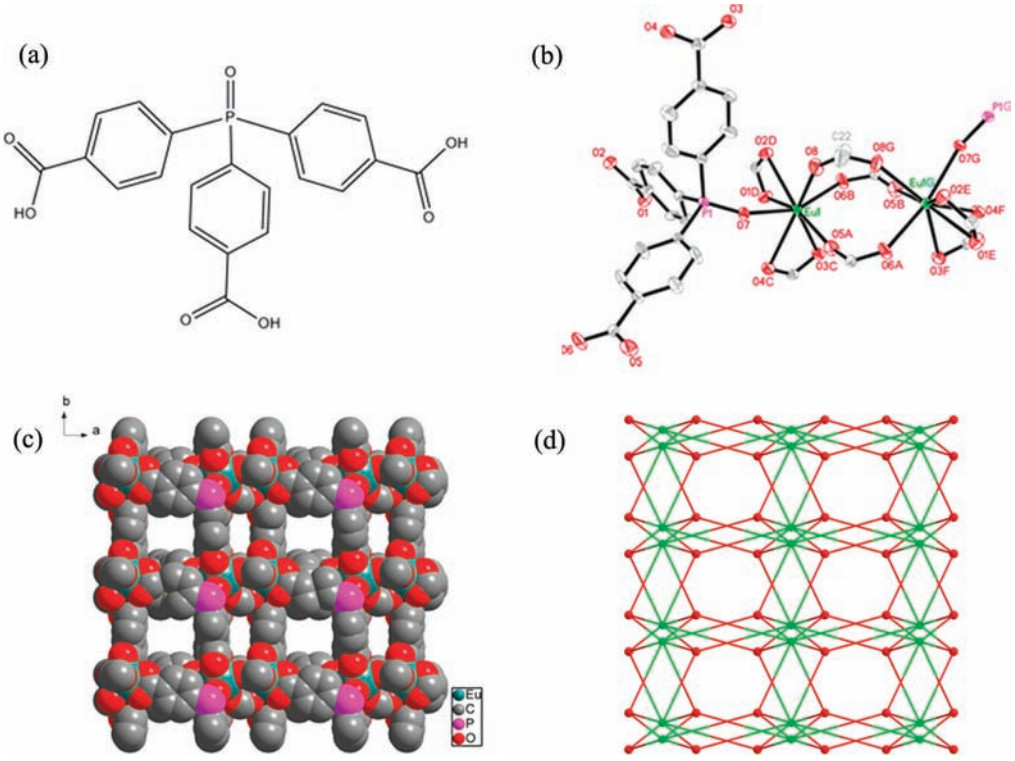

Figure 2. (a) H_3TPO ligand. (b) Coordination environment of compound **3**. (c) Space-filling packing of **3** along [0,0,1] direction. (d) View of (4,8)-connected net. Symmetry transformations used to generate equivalent atoms: A $-x + 1, -y + 1, -z + 1$; B $x, -y + 1, z - {}^1/_2$; C $x, y - 1, z$; D $-x, y, -z + {}^1/_2$; E $1 + x, y, z$; F $1 - x, y - 1, {}^1/_2 - z$; G $-x + 1, y, -z + {}^1/_2$.

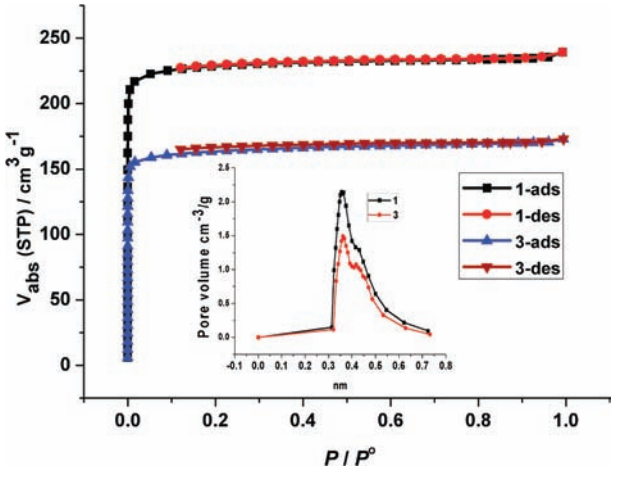

Figure 3. Gas sorption isotherms of N_2. Insert: Horvath−Kawazoe differential pore volume plot of **1** and **3**; ads = adsorption and des = desorption.

those calculated from the structure refined using single-crystal X-ray diffraction. The argon sorption isotherms were collected at 87 K (Figure S8). Again, the sorption isotherms of **1** and **3** showed a typical type-I behavior, albeit the values are slightly lower than those of N_2 adsorption.

The high porosities and surface areas in **1** and **3** prompted us to evaluate their hydrogen adsorption performances. Low-pressure hydrogen sorption isotherms of the desolvated samples at 77 K reveal reversible hydrogen adsorption as shown in Figure 4a. At 77 K and 1 atm, the excess gravimetric hydrogen uptake capacities of **1** and **3** reach to 1.29% and 0.76%, respectively. The H_2 uptake of **1** is lower than the previously reported data for **SNU-21** (1.95%)[17] and is comparable to **IRMOF-2** (1.21%), **IRMOF-9** (1.17%), and **IRMOF-20** (1.37%)[18] under the same measurement conditions. In particular, the H_2 uptake of **1** at 77 K and 1 atm (1.29%) is almost equal to that of Dy(BTC) (1.32%);[5c] both compounds have similar BET surface areas [692 $m^2\ g^{-1}$ for **1** and 655 $m^2\ g^{-1}$ for Dy(BTC)], but the latter has available Lewis-acid metal sites with larger pore sizes (6×6 Å^2). These results indicate that the appropriate pore is beneficial for enhancing adsorption capacities. At 77 K, the samples exhibit an increasing uptake accompanied with the increasing of pressure and the uptake values reach to 2.66% for **1** and 1.58% for **3** at 40 bar (Figure 4b). It is clear that the capacities do not saturate even at 40 bar, anticipating the uptake of more H_2 at higher pressure.

The adsorption isotherms of CO_2 for **1** and **3** were measured up to 1 atm (Figure 5). The CO_2 uptake values for **1** were 66.90 $cm^3\ g^{-1}$ (2.97 mmol g^{-1}) at 273 K and 43.44 $cm^3\ g^{-1}$ (1.93 mmol g^{-1}) at 298 K. The CO_2 uptake for **1** at 273 K is comparable with those of the currently best performing **ZIF-69**[19] (70 $cm^3\ g^{-1}$) under the same measurement conditions (273 K and 1 atm). The CO_2 uptake for **3** was 53.62 $cm^3\ g^{-1}$ (2.39 mmol g^{-1}) at 273 K and 31.76 $cm^3\ g^{-1}$ (1.41 mmol g^{-1}) at 298 K. These values of CO_2 uptake for **1** and **3** are high and comparable with those well examined values in recently reported zeolite frameworks (30−60 $cm^3\ g^{-1}$) under the similar measurement conditions.[19] More interestingly, as shown in Figure 5, both compounds **1** and **3** hardly adsorbed N_2 at ambient temperature (3.03 $cm^3\ g^{-1}$ for **1**, 2.57 $cm^3\ g^{-1}$ for **3** at 273 K and 1 atm; 1.54 $cm^3\ g^{-1}$ for **1**, 1.24 $cm^3\ g^{-1}$ for **3** at 298 K and 1 atm). The CO_2/N_2 selectivities at 273 K and 1 atm are 22.0 for **1** and 20.9 for **3** as calculated from the uptake ratio by volume for CO_2 over N_2, while the values reach to 28.2 for **1** and 25.61 for **3** at 298 K and 1 atm.

The selective CO_2 adsorption over N_2 in **1** and **3** is mainly attributed to the fact that at these temperatures CO_2 is much more condensable than N_2. In addition, the differences in the electrostatic interactions between porous surface and adsorbates also contribute to the excellent selectivity. The recent computational and experimental studies have demonstrated that charged porous framework materials exhibit much stronger binding interactions for CO_2 molecules.[20] The anionic frameworks introduce charges into the host material framework, which can give rise to an electric field interacting with

dx.doi.org/10.1021/ic202082w | Inorg. Chem. 2012, 51, 1813−1820

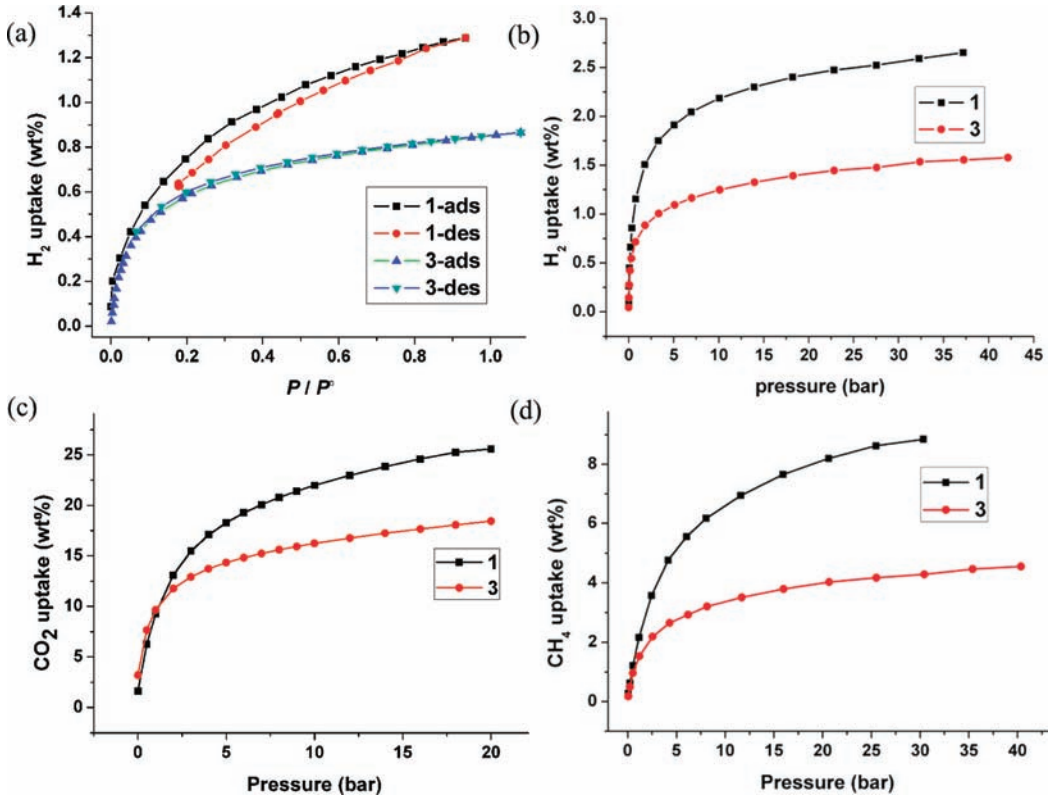

Figure 4. (a) Low-pressure and (b) high-pressure H_2 sorption isotherms for **1** and **3** at 77 K. High-pressure (c) CO_2 and (d) CH_4 sorption isotherms for **1** and **3** at 273 K, respectively; ads = adsorption and des = desorption.

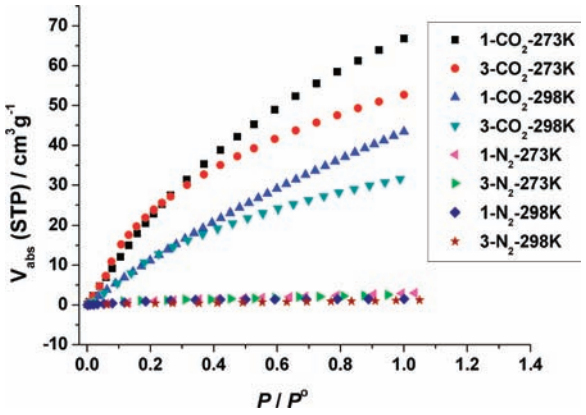

Figure 5. CO_2 and N_2 sorption isotherms of **1** and **3**.

quadrupole molecules. Because the quadrupole moment of CO_2 is larger than that of N_2, the two compounds induce stronger interaction with CO_2 than that with N_2. Besides, the small kinetic diameter of CO_2 (3.30 Å) enables more adsorbing sites to be accessible by CO_2 in the channel; correspondingly, the close similarity of the kinetic diameter of N_2 (3.64 Å) to the channel size of **1** and **3** makes it difficult for N_2 to diffuse into the channel. This molecular sieve effect was also observed in other compounds.[21]

The preferential adsorption of CO_2 over N_2 in **1** and **3** prompted us to evaluate their high-pressure carbon dioxide adsorption performances. As shown in Figure 4c, gravimetric carbon dioxide (CO_2) adsorption isotherms were recorded up to 20 bar at 273 K. At 273 K and 20 bar, the CO_2 uptake is 25.58% and 18.42% for **1** and **3**, respectively. Taking into account the moderate surface areas for **1** and **3**, the CO_2 uptake is quite considerable. To further monitor the general gas storage capacity and behavior, gravimetric methane (CH_4) adsorption isotherms were recorded up to 40 bar at 273 K (Figure 4d). At 40 bar, the CH_4 uptake of **3** is 4.54%, corresponding to a volumetric uptake of 63.6 cm^{-3} g^{-1}. The value of **1** reaches to 8.85%, corresponding to a volumetric uptake of 124 cm^{-3} g^{-1}, lower than that of recently reported **NOTT-140**.[22]

Photoluminescent Investigation. Lanthanide compounds are known for their photoluminescent properties. While being excited at 320 nm at room temperature, H_3TPO ligand exhibits a broad emission band at ~380 nm, which can be ascribed to the intraligand $\pi \rightarrow \pi^*$ transitions (Figure S9). The solid-state emission spectra of **2**, **3**, **5**, and **6** show the characteristic emission bands for corresponding Ln(III) ions, and all of them exhibit excellent luminescent properties with intense and narrow emission bands. When **2** was excited at 290 nm, emissions that appeared in the range 550−800 nm are ascribed to the $^4G_{5/2}-^6H_{5/2,7/2,9/2,11/2}$ transitions (Figure 6a).

Complex **3** displays intense red luminescence and shows the characteristic emission bands for f−f transitions of europium(III) ion when excited at 290 nm (Figure 6b). The strong intensity of emission at 617 nm in the red region is attributed to $^5D_0 \rightarrow {}^7F_2$ transition. The medium strong emission at 592 nm corresponds to the $^5D_0 \rightarrow {}^7F_1$ transition, and the other medium intensity of emission at 700 nm ascribes to $^5D_0 \rightarrow {}^7F_4$ transition. The weak emission bands at 536 and 650 nm arise from the $^5D_0 \rightarrow {}^7F_0$ and $^5D_0 \rightarrow {}^7F_3$ transitions, respectively. The spectrum is dominated by the intense band of the $^5D_0 \rightarrow {}^7F_2$ electron dipole transition, which is the so-called hypersensitive transition and is responsible for the brilliant red emission of these complexes. The quantum yield of complex **3** was determined by means of an integrating sphere, and the value reaches to 43.3%.

As can be seen in Figure 6c, under excitation of 290 nm, complex **5** exhibits characteristic terbium(III) emission bands, resulting from the $^5D_4 \rightarrow {}^7F_J$ (J = 6, 5, 4, 3, and 2) transitions. The emission band at 490 nm arises from the $^5D_4 \rightarrow {}^7F_6$ transition, the strong band at 544 nm is attributed to the $^5D_4 \rightarrow {}^7F_5$ transition, and the band at 587 nm corresponds to the $^5D_4 \rightarrow {}^7F_4$ transition. The band at 621 nm is attributed to the $^5D_4 \rightarrow {}^7F_3$ transition, and the weak band at 650 nm is attributed to the $^5D_4 \rightarrow {}^7F_2$ transition. Surprisingly, the quantum yield

dx.doi.org/10.1021/ic202082w | Inorg. Chem. 2012, 51, 1813−1820

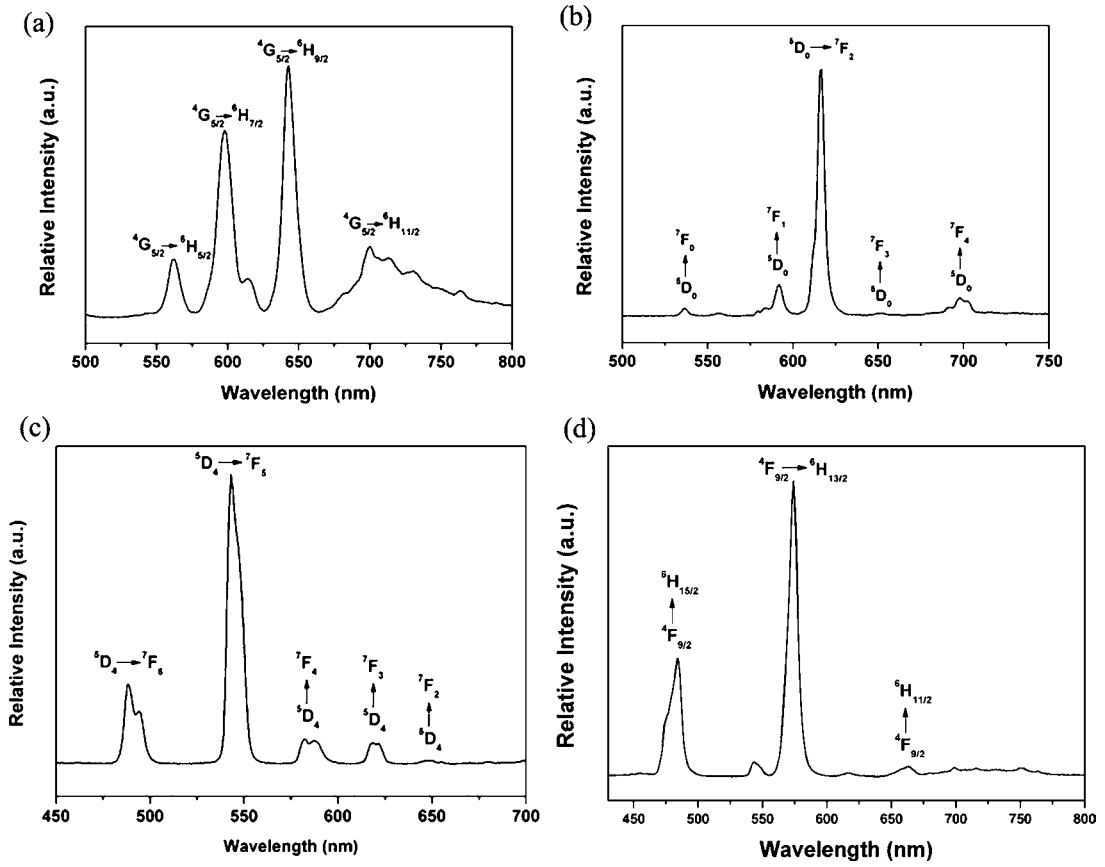

Figure 6. Solid-state photoluminescence spectra of complexes (a) **2**, (b) **3**, (c) **5**, and (d) **6**.

is up to 74.8% under excitation at 290 nm. In some cases, relatively high quantum yields have been reported.[23] However, to the best of our knowledge, only a few good results (Φ > 60%) were obtained in MOFs up to now.[3b]

As shown in Figure 6d, the profiles of the emission bands in the range 450−700 nm for complex **6** are in agreement with previously reported spectra of dysprosium(III) complexes.[5e] Under an excitation of 290 nm, compound **6** displays a strong emission band at 573 nm ($^4F_{9/2} \rightarrow {}^6H_{13/2}$), an emission band at 480 nm ($^4F_{9/2} \rightarrow {}^6H_{15/2}$) with a much lower intensity, and a very weak band at 662 nm ($^4F_{9/2} \rightarrow {}^6H_{11/2}$).

CONCLUSION

In summary, a series of lanthanide MOFs formulated as $[Ln_2(TPO)_2(HCOO)]\cdot(Me_2NH_2)\cdot(DMF)_4\cdot(H_2O)_6$ {Ln = Y (**1**), Sm (**2**), Eu (**3**), Gd (**4**), Tb (**5**), Dy (**6**), Ho (**7**), Er (**8**), Tm (**9**), Yb (**10**), and Lu (**11**); H_3TPO = tris(4-carboxylphenyl)phosphineoxide; DMF = *N*,*N*-dimethylformamide} were prepared under microwave conditions rapidly and efficiently, and their photoluminescence spectra and gas adsorption properties were investigated. Compounds **1** and **3** retain structural integrity and permanent microporosity after guest removal, with good capability of gas adsorption for hydrogen, carbon dioxide, and methane. Furthermore, the resulting compounds show high and preferential CO_2 adsorption over N_2 at room temperature, indicating that the present materials can be applied in a CO_2 capture process.

ASSOCIATED CONTENT

Supporting Information

Powder X-ray diffraction patterns, TGA curves, ^1H NMR spectra, the solid excitation and emission spectra of H_3TPO, and tables of selected bond distances and angles for complexes **1**−**11**. This material is available free of charge via the Internet at http://pubs.acs.org.

AUTHOR INFORMATION

Corresponding Author

*E-mail: rcao@fjirsm.ac.cn. Phone: +86-591-83725186. Fax: +86-591-83796710.

ACKNOWLEDGMENTS

We are grateful for financial support from 973 Program (2011CB932504, 2012CB821705), 863 Program (2011AA03A407), NSFC (20731005, and 91022007), Fujian Key Laboratory of Nanomaterials (2006L2005), and the Key Project from CAS.

REFERENCES

(1) Kitagawa, S.; Kitaura, R.; Noro, S.-i. *Angew. Chem., Int. Ed.* **2004**, *43*, 2334−2375.

(2) (a) Morris, R. E.; Wheatley, P. S. *Angew. Chem., Int. Ed.* **2008**, *47*, 4966−4981. (b) Hong, D. Y.; Hwang, Y. K.; Serre, C.; Ferey, G.; Chang, J. S. *Adv. Funct. Mater.* **2009**, *19*, 1537−1552. (c) Natarajan, S.; Mahata, P. *Chem. Soc. Rev.* **2009**, *38*, 2304−2318. (d) Li, J.-R.; Ma, Y.; McCarthy, M. C.; Sculley, J.; Yu, J.; Jeong, H.-K.; Balbuena, P. B.; Zhou, H.-C. *Coord. Chem. Rev.* **2011**, *255*, 1791−1823.

(3) (a) Maji, T. K.; Mostafa, G.; Chang, H.-C.; Kitagawa, S. *Chem. Commun.* **2005**, *41*, 2436−2438. (b) Lin, Z. J.; Xu, B.; Liu, T. F.; Cao, M. N.; Lu, J. A.; Cao, R. *Eur. J. Inorg. Chem.* **2010**, 3842−3849.

(4) Rocha, J.; Carlos, L. D.; Paz, F. A. A.; Ananias, D. *Chem. Soc. Rev.* **2011**, *40*, 926−940.

(5) (a) Devic, T.; Serre, C.; Audebrand, N.; Marrot, J.; Ferey, G. *J. Am. Chem. Soc.* **2005**, *127*, 12788−12789. (b) Rosi, N. L.; Kim, J.;

Eddaoudi, M.; Chen, B. L.; O'Keeffe, M.; Yaghi, O. M. *J. Am. Chem. Soc.* **2005**, *127*, 1504−1518. (c) Guo, X. D.; Zhu, G. S.; Li, Z. Y.; Sun, F. X.; Yang, Z. H.; Qiu, S. L. *Chem. Commun.* **2006**, *42*, 3172−3174. (d) Park, Y. K.; Choi, S. B.; Kim, H.; Kim, K.; Won, B. H.; Choi, K.; Choi, J. S.; Ahn, W. S.; Won, N.; Kim, S.; Jung, D. H.; Choi, S. H.; Kim, G. H.; Cha, S. S.; Jhon, Y. H.; Yang, J. K.; Kim, J. *Angew. Chem., Int. Ed.* **2007**, *46*, 8230−8233. (e) Ma, S. Q.; Yuan, D. Q.; Wang, X. S.; Zhou, H. C. *Inorg. Chem.* **2009**, *48*, 2072−2077. (f) Jiang, H. L.; Tsumori, N.; Xu, Q. *Inorg. Chem.* **2010**, *49*, 10001−10006. (g) Lee, W. R.; Ryu, D. W.; Lee, J. W.; Yoon, J. H.; Koh, E. K.; Hong, C. S. *Inorg. Chem.* **2010**, *49*, 4723−4725. (h) Guo, Z.; Xu, H.; Su, S.; Cai, J.; Dang, S.; Xiang, S.; Qian, G.; Zhang, H.; O'Keeffe, M.; Chen, B. *Chem. Commun.* **2011**, *47*, 5551−5553.

(6) de la Hoz, A.; Diaz-Ortiz, A.; Moreno, A. *Chem. Soc. Rev.* **2005**, *34*, 164−178.

(7) Hu, Y. Y.; Liu, C.; Zhang, Y. H.; Ren, N.; Tang, Y. *Microporous Mesoporous Mater.* **2009**, *119*, 306−314.

(8) (a) Gass, I. A.; Milios, C. J.; Whittaker, A. G.; Fabiani, F. P. A.; Parsons, S.; Murrie, M.; Perlepes, S. P.; Brechin, E. K. *Inorg. Chem.* **2006**, *45*, 5281−5283. (b) Milios, C. J.; Vinslava, A.; Whittaker, A. G.; Parsons, S.; Wernsdorfer, W.; Christou, G.; Perlepes, S. P.; Brechin, E. K. *Inorg. Chem.* **2006**, *45*, 5272−5274. (c) Millos, C. J.; Gavin Whittaker, A.; Brechin, E. K. *Polyhedron* **2007**, *26*, 1927−1933. (d) Zhang, S.-H.; Song, Y.; Liang, H.; Zeng, M.-H. *CrystEngComm* **2009**, *11*, 865−872. (e) Zhang, S.-H.; Tang, M.-F.; Ge, C.-M. *Z. Anorg. Allg. Chem.* **2009**, *635*, 1442−1446.

(9) (a) Ni, Z.; Masel, R. I. *J. Am. Chem. Soc.* **2006**, *128*, 12394−12395. (b) Jhung, S. H.; Lee, J. H.; Yoon, J. W.; Serre, C.; Ferey, G.; Chang, J. S. *Adv. Mater.* **2007**, *19*, 121−124. (c) Seo, Y. K.; Hundal, G.; Jang, I. T.; Hwang, Y. K.; Jun, C. H.; Chang, J. S. *Microporous Mesoporous Mater.* **2009**, *119*, 331−337. (d) Xiang, Z. H.; Cao, D. P.; Shao, X. H.; Wang, W. C.; Zhang, J. W.; Wu, W. Z. *Chem. Eng. Sci.* **2010**, *65*, 3140−3146. (e) Klinowski, J.; Almeida Paz, F. A.; Silva, P.; Rocha, J. *Dalton Trans.* **2011**, *40*, 321−330.

(10) (a) Jhung, S. H.; Lee, J.-H.; Forster, P. M.; Férey, G.; Cheetham, A. K.; Chang, J.-S. *Chem.—Eur. J.* **2006**, *12*, 7899−7905. (b) Lin, Z.; Wragg, D. S.; Morris, R. E. *Chem. Commun.* **2006**, *42*, 2021−2023. (c) Amo-Ochoa, P.; Givaja, G.; Miguel, P. J. S.; Castillo, O.; Zamora, F. *Inorg. Chem. Commun.* **2007**, *10*, 921−924. (d) Liu, W. L.; Ye, L. H.; Liu, X. F.; Yuan, L. M.; Lu, X. L.; Jiang, J. X. *Inorg. Chem. Commun.* **2008**, *11*, 1250−1252. (e) Silva, P.; Valente, A. A.; Rocha, J.; Paz, F. A. A. *Cryst. Growth Des.* **2010**, *10*, 2025−2028.

(11) (a) Humphrey, S. M.; Oungoulian, S. E.; Yoon, J. W.; Hwang, Y. K.; Wise, E. R.; Chang, J.-S. *Chem. Commun.* **2008**, *44*, 2891−2893. (b) Bohnsack, A. M.; Ibarra, I. A.; Hatfield, P. W.; Yoon, J. W.; Hwang, Y. K.; Chang, J.-S.; Humphrey, S. M. *Chem. Commun.* **2011**, *47*, 4899−4901. (c) Gao, Q.; Wu, M.-Y.; Chen, L.; Jiang, F.-L.; Hong, M.-C. *Inorg. Chem. Commun.* **2009**, *12*, 1238−1241.

(12) Molecular Structure Corporation and Rigaku. *CrystalClear, Version 1.36*;. MSC: The Woodlands, TX, and Rigaku Corporation: Tokyo, Japan, 2000

(13) Sheldrick, G. M. *SHELXS-97, Program for Crystal Structure Solution and Refinement*; University of Göttingen: Gottingen, Germany, 1997.

(14) Spek, A. L. *J. Appl. Crystallogr.* **2003**, *36*, 7.

(15) Blatov, V. A. *IUCr CompComm. Newsletter* **2006**, *7*, 4. See also http://www.topos.ssu.samara.ru/.

(16) Burrows, A. D.; Cassar, K.; Duren, T.; Friend, R. M. W.; Mahon, M. F.; Rigby, S. P.; Savarese, T. L. *Dalton Trans.* **2008**, 2465−2474.

(17) Kim, T. K.; Suh, M. P. *Chem. Commun.* **2011**, *47*, 4258−4260.

(18) Rowsell, J. L. C.; Yaghi, O. M. *J. Am. Chem. Soc.* **2006**, *128*, 1304−1315.

(19) Banerjee, R.; Furukawa, H.; Britt, D.; Knobler, C.; O'Keeffe, M.; Yaghi, O. M. *J. Am. Chem. Soc.* **2009**, *131*, 3875−3877.

(20) (a) Liu, D.; Zhong, C. *J. Mater. Chem.* **2010**, *20*, 10308−10318. (b) Xu, Q.; Liu, D. H.; Yang, Q. Y.; Zhong, C. L.; Mi, J. G. *J. Mater. Chem.* **2010**, *20*, 706−714.

(21) Hou, L.; Shi, W.-J.; Wang, Y.-Y.; Guo, Y.; Jin, C.; Shi, Q.-Z. *Chem. Commun.* **2011**, *47*, 5464−5466.

(22) Tan, C.; Yang, S.; Champness, N. R.; Lin, X.; Blake, A. J.; Lewis, W.; Schroder, M. *Chem. Commun.* **2011**, *47*, 4487−4489.

(23) Fiedler, T.; Hilder, M.; Junk, P. C.; Kynast, U. H.; Lezhnina, M. M.; Warzala, M. *Eur. J. Inorg. Chem.* **2007**, 291−301.